Applied Geochemistry 95 (2018) 85–96

Contents lists available at ScienceDirect

Applied Geochemistry

journal homepage: www.elsevier.com/locate/apgeochem

Influence of colloids on metal concentrations and radiogenic strontium isotopes in groundwater and oil and gas-produced waters

Thai T. Phan[a,b,c,*], J. Alexandra Hakala[a], Daniel J. Bain[b]

[a] National Energy Technology Laboratory, U.S. Department of Energy, Pittsburgh, PA 15236, USA
[b] Department of Geology and Environmental Science, University of Pittsburgh, Pittsburgh, PA 15260, USA
[c] Department of Earth and Environmental Sciences, University of Waterloo, ON, N2L 3G1, Canada

ARTICLE INFO

Editorial handling by Thomas H. Darrah

Keywords:
Colloids
Colloidal clays
Geochemical tracers
Strontium isotopes
Lithium isotopes
Marcellus shale
Groundwater
Produced water

ABSTRACT

Concentrations and isotopic compositions of Li and Sr can be used to identify water-rock interactions and fluid mixing in petroleum reservoirs, such as mixing between hydraulic fracturing fluid and *in-situ* formation water in hydraulically fractured shales. However, the physical changes during mixing in the subsurface environment and during collection of produced water are not clear. We hypothesize that the colloidal particles potentially affect measured constituents in produced waters and degrade the utility of Li and Sr isotopes as geochemical tracers of fluid sources and water-rock interactions. Therefore, this study investigated the influence of colloids on the metal concentrations and isotopes (δ^7Li and $^{87}Sr/^{86}Sr$) by analyzing water that was filtered through successively smaller membranes (0.45 μm, 0.2 μm, and 3 kDa). We found that the differences in the concentrations of major and most minor elements (B, Ca, Ga, K, Li, Mg, Na, Ga, Rb, and Sr) in the < 0.45 μm, the < 0.2 μm, and the < 3 kDa fractions of groundwater and oil produced water are not statistically different ($p > 0.05$; Student's t-test). Likewise, similar results were observed for the < 0.45 μm, the < 0.2 μm-centrifuged, and the < 3 kDa fractions of gas produced water. In the < 0.45 μm fraction of groundwater, U is up to 8% greater than U in the 3 kDa fraction, possibly due to complexation of U with natural organic matter. The formation of Fe oxyhydroxides during sample collection was observed in all three types of waters, however does not significantly affect the measured $^{87}Sr/^{86}Sr$ between three fractions of the study waters. On the other hand, Al, Si, and Ti are enriched in the < 0.45 μm fraction relative to the < 3 kDa fraction of gas produced water, likely due to aluminosilicate minerals (e.g., clays and quartz). However, interactions of Sr and Li with these minerals do not result in statistically significant differences ($p > 0.05$) in $^{87}Sr/^{86}Sr$ among three fractions of groundwater and both oil and gas produced waters. Similarly, no difference in δ^7Li in < 0.45 μm and < 0.2 μm-centrifuged fractions of gas produced water was observed. Ultimately, overestimated concentration data of Al, Si, and Ti in water filtered through a 0.45 μm membrane due to the presence of colloidal clays can create misinterpretations of chemical water-rock interactions in hydraulically fractured shale in the subsurface.

1. Introduction

Naturally-occurring isotopes of metals such as Li, B, and Sr, are applied as geochemical tracers of biogeochemical reactions in geologic systems, and of fluid mixing between geologic units (Capo et al., 2014; Phan et al., 2016; Warner et al., 2014). Knowledge of how sampling protocols affect dissolved geochemical indicators, such as those of the metal isotopes and other trace metals, is important for ensuring the sample undergoing analysis represents solution chemistry. This includes confidence in knowing whether the measured tracer is associated with a fluid-based process (fluid mixing; biogeochemical interaction), is part of reservoir rock erosion, or is changed due to formation of insoluble species in solution during sampling.

Produced water chemistry provides useful information about borehole conditions critical for field operations, and wastewater management associated with onshore unconventional oil and gas resources (Arthur et al., 2005). For example, chemical and isotopic compositions such as Li (δ^7Li) and radiogenic Sr ($^{87}Sr/^{86}Sr$) isotopes are useful indicators of the temporal evolution of produced water (Capo et al., 2014; Phan et al., 2016; Rowan et al., 2015; Warner et al., 2014), oil sands process-affected water (Harkness et al., 2018), and water-rock interactions in the subsurface (Bottomley et al., 1999; Humez et al., 2014). Hydraulic fracturing technology involves multi-stage injection of large quantities of fracturing fluid at high pressure to create fractures in the host rock (Hubbert and Willis, 1972). The local energy from high shear

* Corresponding author. Department of Earth and Environmental Sciences, University of Waterloo, 200 University Ave. W, Ontario, N2L 3G1, Canada.
E-mail addresses: thai.phan@uwaterloo.ca, thaiphan@pitt.edu (T.T. Phan).

https://doi.org/10.1016/j.apgeochem.2018.05.018
Received 7 February 2018; Received in revised form 2 May 2018; Accepted 23 May 2018
Available online 25 May 2018
0883-2927/

stresses acting on shale during micro-fracturing process produces particles (Bažant et al., 2014) of undetermined size and mineralogical compositions. Colloids associated with physical erosion of reservoir rock therefore also may be present in produced waters.

Metals in aquatic environments exist in a complex mixture of phases including truly dissolved ionic forms, colloidal, and particulate phases (Lead and Wilkinson, 2006). Colloids are ubiquitous in natural waters, particularly aluminosilicate colloids, and can be a significant carrier of many potentially toxic metals and radionuclides in water (Kretzschmar et al., 1999; Kretzschmar and Schäfer, 2005; Trostle et al., 2016). For example, complexation with dissolved organic matter and inorganic colloidal material is a key influence on the transport of transition metals, rare earth elements, and uranium in stream water in Marshall Gulch, Santa Catalina Mountains Critical Zone Observatory (Trostle et al., 2016). However, the role of colloid transport of metals and radionuclides in waters with unusual chemical composition (Chapman et al., 2012; Rowan et al., 2015) co-produced with oil and natural gas from petroleum reservoirs is poorly documented.

Although most fluid sampling protocols consider 0.45 μm an appropriate size cutoff to separate dissolved versus colloidal material (Engle et al., 2016; Harkness et al., 2018; Kharaka et al., 1987; Phan et al., 2016; Pfister et al., 2017; Rowan et al., 2015; Zhang et al., 2015), it is possible that naturally-occurring colloids, such as clays and Fe oxides, smaller than 0.45 μm (Filella, 2007) are present and influence metal geochemical behavior. For instance, δ^7Li in clays (−1.5 to +5.0‰; Chan et al., 2006) are generally lower than δ^7Li values in surface water (e.g., δ^7Li values in the dissolved load of Amazon river basin = +1.2‰ to +32.9‰; Dellinger et al., 2015). Thus, δ^7Li in 0.45 μm filtered water containing colloidal clays would be likely lower than the δ^7Li in the dissolved load. In addition, previous studies showed that Sr can be redistributed in the water column due to the transport of Fe aggregates in which Sr is co-precipitated and adsorbed (Andersson et al., 1994; Wortberg et al., 2017). This colloidal transport of Sr can degrade the conservative behavior of Sr isotopes as a tracer of fluid mixing (Andersson et al., 1994) when the Sr associated with colloids is significant relative to truly dissolved Sr and has distinctive isotopic composition. Consequently, elemental and isotopic data measured in samples filtered through 0.45 μm membrane can potentially lead to misinterpretations of chemical interactions between water and reservoir rock, and poor outcomes in geochemical modeling. Such misinterpretations include an over-estimation of truly dissolved species when the metal is present due to physical erosion of material from the shale, or an under-estimation of truly dissolved species if the metal adsorbs or co-precipitates with newly-formed colloids and is not properly concentrated as part of analytical pre-treatment procedures.

This study investigates the presence and effect of small colloids (pass through 0.45 μm membrane, but retains on 3 kDa membrane) on both major and trace metal contents, and isotopic compositions of Sr in three types of environmental waters: fluvial and lacustrine clastic groundwater, produced water from oil-bearing dolostone (oil produced water), and produced water from gas-bearing clay-rich shale (gas produced water). We focus our discussion on the role of both colloids formed during sample collection (sampling artifacts) and naturally occurring colloids in controlling the enrichment of metals in groundwater, and oil and gas produced waters. Furthermore, the efficacy of Sr as a geochemical tracer and limitations in using geochemical data for interpreting water-rock interactions are also investigated. In addition to Sr isotopes, select produced water samples from gas-bearing formation were also analyzed for Li isotopes to determine whether clay-rich particles, if present, affect the isotopic composition of Li.

2. Methods

2.1. Study area and sample collection

Three different types of water were examined in this study. Groundwater and oil produced water samples were collected at two enhanced oil recovery field sites: East Seminole Field in Gaines County and Emma Field in Andrews County, Texas, USA (Fig. 1) during a May 2016 sampling campaign. Gas produced water samples were collected from one Marcellus Shale gas well in Monongalia County, WV, USA (Fig. 1).

2.1.1. Oil produced water and groundwater collection

In this study, oil produced water was collected at the well-heads of oil producing wells tapping the San Andres Platform Carbonate play of the Permian Central Basin Platform (Dutton et al., 2005). The sampling technique employed in this study was modified after Kharaka et al. (1987), a method widely used for sampling oil and gas produced water (Engle et al., 2016; Pfister et al., 2017; Rowan et al., 2015). Oil produced water samples (n = 14) were collected from 14 oil producing wells from two sites: nine wells from East Seminole Field in the west central area of Gaines County, TX, USA, and five wells from Emma Field in Andrews County, TX, USA (Fig. 1). One sample was collected from each well. Briefly, the oil produced water was allowed to sit in a carboy for at least an hour to allow separation of the water and oil. Water was withdrawn via a spigot at the base of the carboy and passed through a glass wool-packed syringe to additionally adsorb oil and minimize atmospheric exposure. The sample then was filtered through 0.45 μm high capacity filter (EnviroTech GWE) under gravity into acid-washed Nalgene HDPE bottles. Water that passed through the system during the first minute was discarded before collecting the actual sample. We assume that a one-minute rinse is enough for adsorption to reach equilibrium and, thus, no loss of ions occurs during the collection of actual water sample. The filtered sample (< 0.45 μm fraction) was further syringe-filtered through 0.2 μm membrane into acid-washed Nalgene HDPE bottles (< 0.2 μm fraction).

Groundwater from the Ogallala aquifer was collected from either residential wells or agricultural irrigation wells (Fig. 1) in May 2016. One sample was collected from each well: five wells in the East Seminole Field and one well in the Emma Field. Stagnant water in the pipeline was flushed for about 3–5 min before rinsing and collecting the groundwater sample into a two-gallon water jug with spigot. Groundwater was collected following the above procedure, but without glass wool unit filtration. The < 0.45 μm and < 0.2 μm fractions were preserved by acidification on site using ultrapure HNO_3 (Optima® grade, Thermo Fisher). For groundwater and oil produced water, a separate, unacidified, and no-headspace HDPE bottle containing the < 0.45 μm fraction water was preserved on ice during transport to the laboratory. Within a week, these unacidified fraction waters were further filtered through a 3 kDa (~2 nm pore size) molecular weight cutoffs membrane (EMD Millipore) by centrifugation at 5000 rpm for 30 min (< 3 kDa fraction) in the laboratory.

2.1.2. Gas produced water collection

The natural gas produced water samples were collected from a hydraulically fractured Marcellus Shale gas well (Well MIP-3H) at the Marcellus Shale Energy and Environment Laboratory (MSEEL) field site in Monongalia County (Morgantown, WV, USA). The samples (n = 16) were collected during the two-month period following the first day when flowback water returned to the well head. A slightly different

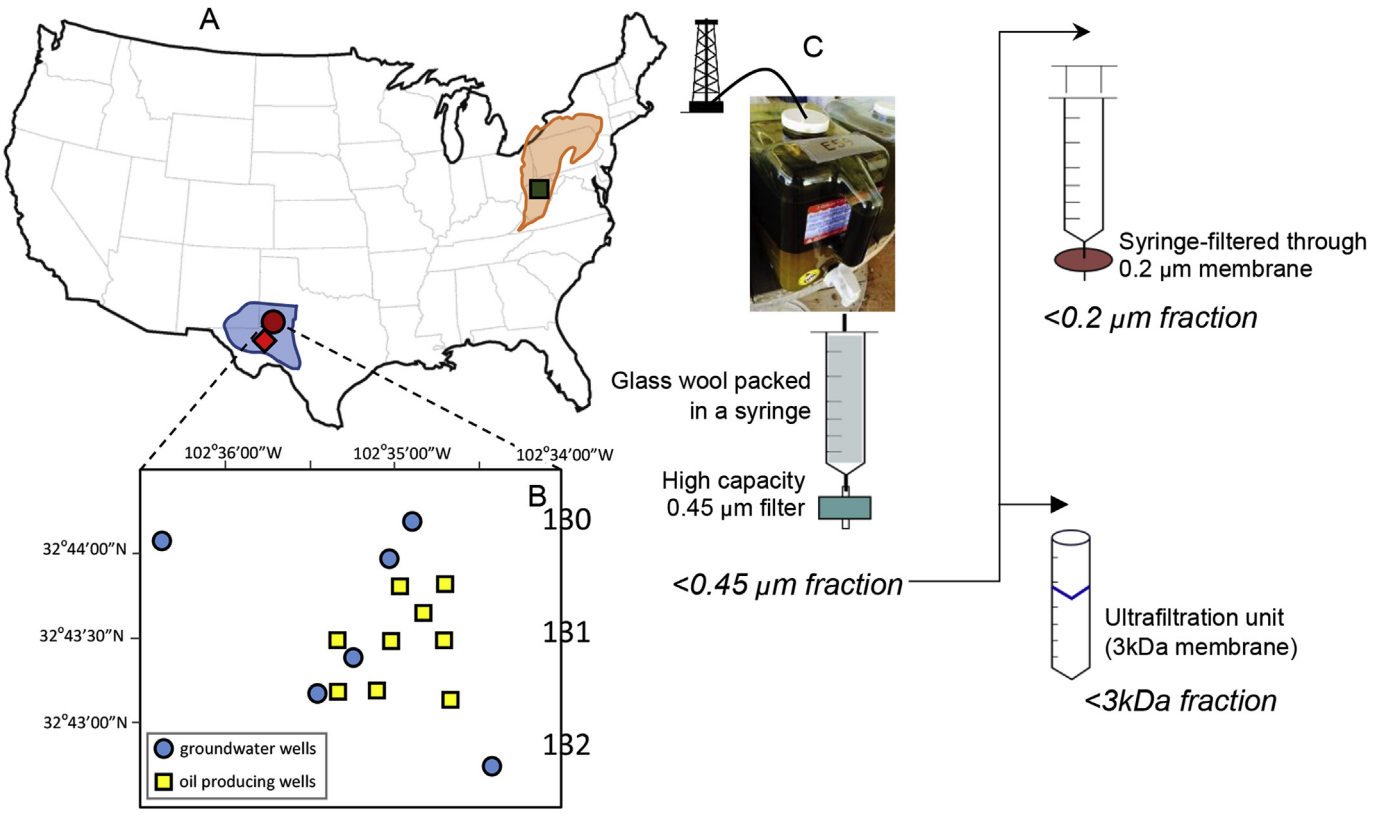

Fig. 1. Locations (A) of analyzed water samples. Groundwater (n = 7) and oil produced water (n = 14) were collected from residential wells and oil wells, respectively, at East Seminole Field in Gaines County (filled circle) with well locations (B) and Emma Field in Andrews County (filled diamond) in Permian Basin (blue shade), Texas, USA. Gas produced water samples (n = 16) were collected from one hydraulically fractured well targeting Marcellus Shale (orange shade) at Marcellus Shale Energy and Environment Laboratory field site in Morgantown, West Virginia, USA (filled rectangle). Schematic sampling procedure (C), the sample collection and filtration techniques for each water sample type are described in detail in Section 2.1. (For interpretation of the references to color in this figure legend, the reader is referred to the Web version of this article.)

procedure was used compared to the oil produced water samples. The < 0.45 µm fraction water was collected following the procedure above and acidified on site using ultra-pure nitric acid. However, the 0.2 µm-filtered water (unacidified) was stored at 4 °C for up to two months depending on the collection time. Particles of Fe oxy-hydroxide in orange color were found as dispersed colloids and aggregates on the bottom of the sample containers. To evaluate whether precipitation of large particles of Fe oxyhydroxide affects the concentrations of other metals and fractionates the isotopic composition of Sr in the remaining fluid, Fe aggregates were centrifuged and discarded. The remaining supernatant is referred to as < 0.2 µm-centrifuged fraction. An aliquot of this supernatant containing dispersed Fe colloids was further passed through the ultrafiltration unit. The permeate is referred to as the < 3 kDa fraction. Both < 0.2 µm-centrifuged and < 3 kDa fractions were acidified using ultrapure nitric prior to analysis.

2.2. Analytical techniques

Acidified samples were measured for a suite of metal concentrations (Ag, Al, As, B, Ba, Ca, Cr, Cu, Fe, Ga, K, Li, Mg, Mn, Mo, Na, Ni, Rb, Se, Si, Sr, Ti, U, V, Zn) at the University of Pittsburgh on a PerkinElmer NexION 300X ICP-MS using kinetic energy discrimination (KED) mode. Indium was used as an internal standard for correction of matrix effect. In addition, three fractions (< 0.45 µm, < 0.2 µm, and < 3 kDa) of each sample were diluted by similar dilution factors and measured consecutively to ensure consistency in sample preparation and analysis, allowing comparison of the differences between three fractions. Although the accuracy of elemental data was within 10% based on repeated analysis of two groundwater reference standards (NIST1640a and SCP ESL-2), the analytical precision, generally less than 2%, is more important for this study because we compare the difference among fractions of the same samples. The concentration and relative standard deviation (RSD, %), analytical precision, of the analyzed elements are reported in Table S1. All dilution steps including acidification were done gravimetrically. Thus, concentrations of metals (µg/L) reported in Table S1 account for the specific gravity of the samples which was measured by a pycnometer. Note that the uncertainty of specific gravity measurement does not affect the comparison of the concentrations in three fractions because the concentrations were multiplied by a constant value (specific gravity). The total organic carbon (TOC) concentration in < 0.45 µm and < 0.2 µm fractions were analyzed within 2 weeks of collection using a Shimadzu TOC-L following the protocol for

non-purgeable organic carbon. The standard deviation of the analyses performed with the TOC-L was within 1% for TOC values greater than 2 mg/L and within 2% for samples with TOC lower than 2 mg/L. Water samples were analyzed for Li ($^{7}Li/^{6}Li$) and radiogenic Sr ($^{87}Sr/^{86}Sr$) isotopes following the procedures reported in Phan et al. (2016) and Wall et al. (2013), respectively. The isotope compositions were measured by the Neptune Plus multi-collector ICP-MS. The measured $^{7}Li/^{6}Li$ ratio is expressed as per mil deviation from a standard as

$$\delta^{7}Li = (^{7}Li/^{6}Li_{sample}/^{7}Li/^{6}Li_{LSVEC} - 1) \times 1000 \quad (1)$$

where $^{7}Li/^{6}Li_{LSVEC}$ is the average $^{7}Li/^{6}Li$ ratio of SRM-8545 (LSVEC) standard measured before and after the sample. Generally, repeated measurement of LSVEC following the sample standard bracketing convention yields 2SD of $\delta^{7}Li \leq 0.5‰$. For all samples analyzed for $\delta^{7}Li$, the recovery from chromatographic separation of Li from the matrix was > 99% (Phan et al., 2016) to ensure that Li isotopes are not fractionated during column separation (Košler et al., 2001). Measured $\delta^{7}Li$ of an in-house standard (WA-A25; produced water) in this study yielded $\delta^{7}Li = 9.4$ (n = 1) which is consistent with our previous work (9.5 ± 0.4, n = 5; Phan et al., 2016; 9.4 ± 0.1, n = 2; Macpherson et al., 2014). Repeated analysis of an in-house standard (UD6-120518-S; produced water) yielded $^{87}Sr/^{86}Sr = 0.719959 \pm 0.000033$ (2SD; n = 15) which agrees well with our previously reported values: 0.719958 ± 0.000020 (2SD; n = 9)(Phan et al., 2018). Likewise, analysis of a USGS standard (EN-1; Tridacna shell) yielded $^{87}Sr/^{86}Sr = 0.709163 \pm 0.000023$ (2SD; n = 16), consistent with 0.709159 ± 0.000032 (n = 9)(Phan et al., 2018).

2.3. Statistical analysis

To determine the statistical significance of the differences in elemental concentrations, Sr isotopes ($^{87}Sr/^{86}Sr$), and Li isotopes ($\delta^{7}Li$) among the three fractions, we used a Student's t-test at $p \leq 0.05$. It is noted that the sample size used in this study is not large enough to confirm a normal distribution and other requirements for *t*-test. Thus, the discussion based on statistical results is only valid with the assumption that our data meet the *t*-test requirements. To facilitate the comparison, we normalized concentrations of elements in the < 0.45 µm and the < 0.2 µm fractions to the concentration measured in the < 3 kDa fraction. For example, $Li_{(<0.45\ \mu m)}/Li_{(<3kDa)}$ denotes the ratio of Li concentration in the < 0.45 µm fraction over the < 3 kDa fraction. The standard deviation of a ratio of element X is calculated following the equation below.

$$SD\left(\frac{X_{(<0.45\mu m)}}{X_{(<3kDa)}}\right) = \left(\frac{X_{(<0.45\mu m)}}{X_{(<3kDa)}}\right) \cdot \sqrt{\left(\frac{SD(X_{(<0.45\mu m)})}{X_{(<0.45\mu m)}}\right)^{2} + \left(\frac{SD(X_{(<3kDa)})}{X_{(<3kDa)}}\right)^{2}} \quad (2)$$

One-sample *t*-test was used to compare the mean of the two ratios with one (i.e., identical concentrations) and determine if the enrichment of metal concentrations related to colloids found in the < 0.45 µm fraction and the < 0.2 µm fraction is significantly different from one ($p^{*} < 0.05$ in Table 1). In addition, the significance of the differences between the enrichment of elements due to different colloid size classes was examined. First an F-test was used to determine if the variances of the two populations were equal, and then the appropriate *t*-test was selected ($p^{**} < 0.05$ in Table 1). For instance, element X with $p^{**} < 0.05$ means that the difference of the means of $X_{(<0.45\mu m)}/X_{(<3kDa)}$ and $X_{(<0.2\mu m)}/X_{(<3kDa)}$ is significant. Statistical analysis was performed using both Microsoft Excel 2016 and IBM SPSS Statistics 24. Statistical analysis was performed on raw concentrations to avoid potential errors due to rounding.

3. Results and discussion

3.1. Comparison of metal concentrations in < 0.45 µm, < 0.2 µm, < 0.2 µm-centrifuged, and < 3 kDa fractions

The differences in the concentrations of major (Ca, Mg, Na, K) and minor (Li, B, Ga, Rb, Sr) elements in all three fractions (< 0.45 µm, < 0.2 µm, and < 3 kDa) of groundwater and oil produced water are not significant ($p > 0.05$; Table 1; Fig. 2). Similar results are observed for these same elements in the < 0.45 µm, < 0.2 µm-centrifuged, and < 3 kDa fractions of gas produced water. Because these major and minor elements are present in the water at high levels, potential loss due to adsorption negligibly affects the concentration of these elements in the water. Therefore, the concentrations of these elements measured in the < 0.45 µm fraction may be considered representative of the soluble load concentration. It is noted that the discussion below only considers elements with a statistically significant difference between the three fractions and that the mean ratios are greater than 1.05 (greater than the general analytical error of 5%). For example, although the mean value of $As_{(<0.45\ \mu m)}/As_{(<3kDa)} = 2.68$ (Table 1), the concentration difference between the two fractions is not significant ($p > 0.05$), and therefore As is not discussed in detail.

We observed that the concentrations of Fe in the < 0.45 µm fraction is much greater than in the < 0.2 µm-centrifuged (by a factor of 19, median value) and 3 kDa fractions of gas produced water (Table 1). During the sampling campaign for Marcellus produced water, the dark orange color of Fe particles was observed on the filter membrane during syringe filtration of water collected from the water-gas separator of the well. The Fe oxyhydroxide colloids are formed due to the oxidation by atmospheric oxygen during syringe filtration and during storage of unacidified water sample (sampling artifact). Comparing three fractions, the likely underestimated Fe concentration in the < 0.45 µm fraction is least affected by oxidation due to sampling artifact, thus most closely represents the truly dissolved Fe in the water samples. Additional filtration of sample leads to losing Fe.

Unlike major ions, trace metal concentrations are more sensitive to adsorption and/or co-precipitation (e.g., with Fe oxyhydroxide). We found that U concentration in the < 0.45 µm fraction of groundwater is higher than in the < 3 kDa fraction by as many as 8% (Table 1; $p < 0.05$), about 4% on average (n = 6). Previous studies (Jackson et al., 2005; Lenhart et al., 2000) showed that facilitated transport of U due to complexation with natural organic matter (NOM), such as humic and fulvic acids, is significant in acidic (pH < 6) and low carbonate water. Under circumneutral pH and bicarbonate (HCO_3^-) less than 20% of total anions (Pfister et al., 2017) in Ogallala groundwater, our data showed that neither U or U enrichment ($U_{(<0.45\ \mu m)}/U_{(<3kda)}$) correlates moderately with pH values ($r^2 = 0.38$ and 0.04, respectively; not shown). Assuming the U enrichment in the < 0.45 µm fraction (4% on average) is solely due to complexation with NOM, this study result is consistent with previous results from the column experiments on U-NOM complexation (Artinger et al., 2002). The prior study showed that, under circumneutral pH, < 7.6% of U is transported by humic colloids (Artinger et al., 2002). However, a lower percentage of U-NOM complex (< 2%) in field collected water samples was reported in Ranville et al. (2007). Like U in the < 0.45 µm fraction, U in the < 0.2 µm

Table 1
Statistical analysis (one-sample *t*-test) to compare if the enrichment of metals in colloid and nanoparticle pools is significant (p*). The *t*-test was performed to compare if there is a significant difference between < 0.45 μm/ < 3 kDa and between < 0.2 μm/ < 3 kDa (p**).

Elements	Groundwater								Oil Produced Water			
	< 0.45μm/ < 3 kDa			< 0.2 μm/ < 3 kDa			n	p**	< 0.45μm/ < 3 kDa			< 0.2 μm/ < 3 kDa
	Mean	Median	p*	Mean	Median	p*			Mean	Median	p*	Mean
Ag	–	–	–	–	–	–	–	–	–	–	–	–
Al	–	–	–	–	–	–	–	–	–	–	–	–
As	1.18	1.08	0.118	1.03	0.99	0.597	6	0.221	–	–	–	–
B	1.05	1.04	0.160	1.02	1.01	0.159	7	0.163	1.01	0.99	0.560	1.02
Ba	1.02	1.00	0.879	1.00	1.00	0.365	7	0.355	1.17	1.05	***0.049***	0.98
Ca	0.99	0.99	0.276	0.98	0.98	***0.047***	6	0.396	1.00	1.00	0.284	1.00
Cr	–	–	–	–	–	–	–	–	1.35	1.29	***0.023***	1.33
Fe	2.80	1.54	0.117	2.26	1.24	0.304	7	0.728	1.21	1.16	***0.000***	1.18
Ga	1.00	0.99	0.913	0.97	0.96	0.105	4	0.169	–	–	–	–
K	0.99	0.98	0.513	0.99	0.99	0.532	7	0.914	1.06	1.01	0.055	1.07
Li	1.01	1.01	0.228	1.00	1.01	0.977	7	0.392	1.00	1.00	0.644	1.00
Mg	1.06	1.02	0.359	1.05	1.01	0.403	7	0.908	1.00	1.00	0.931	1.00
Mn	1.03	1.02	0.516	1.04	1.01	0.498	3	0.862	1.04	1.02	***0.048***	1.02
Mo	0.98	0.98	0.184	0.98	1.00	0.385	5	0.962	–	–	–	–
Na	1.00	1.01	0.883	1.00	1.00	1.000	7	0.915	1.00	1.00	0.431	1.00
Ni	–	–	–	–	–	–	–	–	–	–	–	–
Rb	1.00	1.01	0.644	1.00	1.00	0.806	7	0.605	1.01	1.01	0.060	1.01
Si	1.04	1.04	***0.047***	0.98	1.01	0.617	7	0.138	0.94	0.93	0.194	0.95
Sr	1.00	1.00	0.661	1.01	1.01	0.296	7	0.280	1.00	1.00	0.551	1.01
Ti	–	–	–	–	–	–	–	–	0.95	0.96	***0.007***	0.94
U	1.04	1.04	***0.009***	1.04	1.04	***0.036***	6	0.767	–	–	–	–
V	1.03	1.02	0.071	1.02	1.01	0.098	6	0.321	1.03	1.02	***0.014***	1.03
Zn	–	–	–	–	–	–	–	–	–	–	–	–

Elements	Oil Produced Water				Gas Produced Water							
	< 0.2 μm/ < 3 kDa		n	p**	< 0.45μm/ < 3 kDa			< 0.2 μm-centrifuged/ < 3 kDa			n	p**
	Median	p*			Mean	Median	p*	Mean	Median	p*		
Ag	–	–	–	–	2.27	2.44	***0.000***	1.38	1.31	***0.001***	14	***0.0001***
Al	–	–	–	–	17.2	7.56	***0.006***	1.00	0.96	***0.999***	16	***0.0059***
As	–	–	–	–	2.68	1.02	1.387	1.11	0.87	0.101	7	0.268
B	1.02	0.085	14	0.618	0.97	0.97	***0.001***	0.97	1.00	0.228	16	0.930
Ba	1.00	0.670	14	***0.046***	1.01	1.01	0.081	1.00	1.00	0.786	16	0.418
Ca	1.00	0.251	14	0.902	1.04	1.04	***0.003***	1.02	1.01	***0.022***	16	0.235
Cr	1.32	***0.008***	4	0.795	–	–	–	–	–	–	–	–
Fe	1.13	***0.002***	14	0.671	53.8	50.90	***0.000***	6.07	2.20	0.059	16	***0.0003***
Ga	–	–	–	–	1.00	0.99	0.454	0.99	0.98	0.078	16	0.330
K	1.01	***0.046***	14	0.855	1.01	1.01	0.132	1.00	1.01	0.335	16	0.446
Li	1.00	0.760	14	0.452	1.01	1.01	0.202	1.00	1.00	0.858	16	0.377
Mg	1.00	0.760	14	0.921	1.01	1.02	0.206	1.01	1.00	0.289	16	0.744
Mn	1.02	***0.003***	14	0.402	1.02	1.01	0.220	0.99	1.00	0.432	16	0.142
Mo	–	–	–	–	1.42	1.43	***0.000***	1.08	1.01	0.145	13	***0.004***
Na	1.00	0.927	14	0.746	1.01	1.01	0.334	1.00	1.00	0.611	16	0.619
Ni	–	–	–	–	1.19	1.10	0.126	0.94	0.93	0.209	16	0.062
Rb	1.01	0.122	14	0.622	1.00	1.00	0.725	1.00	1.00	0.469	16	0.773
Si	0.94	0.200	14	0.854	1.70	1.69	***0.000***	1.05	1.01	0.222	16	***0.000***
Sr	1.01	***0.043***	14	0.407	1.00	1.00	0.395	1.00	1.00	0.374	16	0.962
Ti	0.93	***0.003***	14	0.552	1.14	1.11	***0.002***	1.00	1.00	0.983	16	***0.002***
U	–	–	–	–	–	–	–	–	–	–	–	–
V	1.03	***0.011***	14	0.890	0.97	0.97	0.015	0.97	0.97	***0.008***	16	0.848
Zn	–	–	–	–	1.14	1.06	***0.005***	1.03	1.04	0.143	16	***0.031***

n = number of samples; - = not available due to the measured concentration below the detection limit.
*This one-sample *t*-test is to compare if the enrichment of each metal associated with colloids passing through 0.45 μm membrane and passing through 0.2 μm membrane is significant by comparing the mean ratio with 1.
**This *t*-test is to compare if the enrichment of each metal associated with colloids passing through 0.45 μm membrane is significantly different with the enrichment of metals associated with colloids passing through 0.2 μm membrane.

Table 2
Isotopic composition of Sr ($^{87}Sr/^{86}Sr$) and Li (δ^7Li) in the < 0.45 μm, < 0.2 μm, and < 3 kDa fractions.

Sample ID	Sample Type	$^{87}Sr/^{86}Sr$					δ^7Li, ‰			
		Rep 1	Rep 2	Rep 3	Mean	± 2SD	Rep 1	Rep 2	Rep 3	± 2SD
< 0.45 μm fraction										
C5-16-05	Groundwater	0.708662	n/m	0.708646	0.708654	0.000023	n/m	n/m	n/m	n/m
C2-16-05	Groundwater	0.708603	0.708603	0.708616	0.708607	0.000015	n/m	n/m	n/m	n/m
C4-16-05	Groundwater	0.708651	0.708660	0.708649	0.708653	0.000011	n/m	n/m	n/m	n/m
C3-16-05	Groundwater	0.708652	0.708654	0.708649	0.708652	0.000005	n/m	n/m	n/m	n/m
C6-16-05	Groundwater	0.708644	0.708650	0.708661	0.708652	0.000017	n/m	n/m	n/m	n/m
A4-16-05	Oil produced water	0.707951	0.707918	0.707941	0.707936	0.000033	n/m	n/m	n/m	n/m
A2-16-05	Oil produced water	0.707924	0.707934	0.707940	0.707932	0.000016	n/m	n/m	n/m	n/m
A1-16-05	Oil produced water	0.707904	0.707889	0.707909	0.707901	0.000020	n/m	n/m	n/m	n/m
A3-16-05	Oil produced water	0.707902	0.707938	0.707916	0.707919	0.000036	n/m	n/m	n/m	n/m
EM6-16-05	Oil produced water	0.708694	0.708693	0.708686	0.708691	0.000009	n/m	n/m	n/m	n/m
3H-1	Gas produced water	0.711112	0.711116	n/m	0.711114	0.000006	9.5	9.7	9.6	0.2
3H-7	Gas produced water	0.710426	n/m	n/m	0.710426	–	10.4	10.1	10.3	0.4
3H-10	Gas produced water	0.711041	n/m	n/m	0.711041	–	n/m	n/m	n/m	n/m
3H-15	Gas produced water	0.711234	n/m	n/m	0.711234	–	n/m	n/m	n/m	n/m
3H-21	Gas produced water	0.711339	n/m	n/m	0.711339	–	n/m	n/m	n/m	n/m
< 0.2 μm fraction (groundwater and oil produced water) and < 0.2 μm-centrifuged fraction (gas produced water)										
C5-16-05	Groundwater	0.708635	0.708655	0.708656	0.708649	0.000024	n/m	n/m	n/m	n/m
C2-16-05	Groundwater	0.708608	0.708614	0.708605	0.708609	0.000010	n/m	n/m	n/m	n/m
C4-16-05	Groundwater	0.708659	0.708653	0.708638	0.708650	0.000022	n/m	n/m	n/m	n/m
C3-16-05	Groundwater	0.708651	0.708642	0.708641	0.708644	0.000012	n/m	n/m	n/m	n/m
C6-16-05	Groundwater	0.708655	0.708647	0.708640	0.708647	0.000015	n/m	n/m	n/m	n/m
A4-16-05	Oil produced water	0.707925	0.707930	0.707929	0.707928	0.000005	n/m	n/m	n/m	n/m
A2-16-05	Oil produced water	0.707910	0.707926	0.707915	0.707917	0.000017	n/m	n/m	n/m	n/m
A1-16-05	Oil produced water	0.707883	0.707883	0.707883	0.707883	0.000000	n/m	n/m	n/m	n/m
A3-16-05	Oil produced water	0.707907	0.707916	0.707909	0.707910	0.000010	n/m	n/m	n/m	n/m
EM6-16-05	Oil produced water	0.708681	0.708686	0.708669	0.708679	0.000017	n/m	n/m	n/m	n/m
3H-1	Gas produced water	0.711094	0.711095	0.711116	0.711102	0.000025	9.5	10.0	9.8	0.7
3H-7	Gas produced water	0.710420	0.710425	0.710459	0.710435	0.000042	10.6	10.5	10.5	0.2
3H-10	Gas produced water	0.711044	0.711084	0.711070	0.711066	0.000040	n/m	n/m	n/m	n/m
3H-15	Gas produced water	0.711217	0.711218	0.711213	0.711216	0.000005	n/m	n/m	n/m	n/m
3H-21	Gas produced water	0.711319	0.711327	0.711316	0.711320	0.000011	n/m	n/m	n/m	n/m
3 kDa Fraction										
C5-16-05	Groundwater	0.708660	0.708648	0.708646	0.708651	0.000015	n/m	n/m	n/m	n/m
C2-16-05	Groundwater	0.708622	0.708605	0.708637	0.708621	0.000032	n/m	n/m	n/m	n/m
C4-16-05	Groundwater	0.708646	0.708655	0.708666	0.708656	0.000020	n/m	n/m	n/m	n/m
C3-16-05	Groundwater	0.708648	0.708667	0.708656	0.708657	0.000019	n/m	n/m	n/m	n/m
C6-16-05	Groundwater	0.708665	0.708658	0.708662	0.708662	0.000007	n/m	n/m	n/m	n/m
A4-16-05	Oil produced water	0.707927	0.707940	0.707928	0.707932	0.000015	n/m	n/m	n/m	n/m
A2-16-05	Oil produced water	0.707934	0.707923	n/m	0.707929	0.000015	n/m	n/m	n/m	n/m
A1-16-05	Oil produced water	0.707889	0.707894	0.707883	0.707889	0.000010	n/m	n/m	n/m	n/m
A3-16-05	Oil produced water	0.707914	0.707919	0.707922	0.707919	0.000008	n/m	n/m	n/m	n/m
EM6-16-05	Oil produced water	0.708686	0.708677	0.708682	0.708682	0.000009	n/m	n/m	n/m	n/m
3H-01	Gas produced water	0.711098	0.711099	0.711097	0.711098	0.000003	n/m	n/m	n/m	n/m
3H-07	Gas produced water	0.710432	0.710427	0.710434	0.710431	0.000007	n/m	n/m	n/m	n/m
3H-10	Gas produced water	0.711074	0.711071	0.711071	0.711072	0.000003	n/m	n/m	n/m	n/m
3H-15	Gas produced water	0.711239	0.711228	0.711235	0.711234	0.000011	n/m	n/m	n/m	n/m
3H-21	Gas produced water	0.711335	0.711336	0.711334	0.711335	0.000002	n/m	n/m	n/m	n/m

n/m: not measured.

fraction of groundwater is also greater than in < 3 kDa fraction, though the difference is not significant. This suggests that U is either associated with naturally occurring colloids passing through the 0.2 μm membrane that are removed during ultrafiltration, or that U loss occurs by adsorption onto Fe colloids in the < 0.2 μm fraction. There was no (poor; $r^2 = 0.12$; n = 6; p > 0.05) correlation between U enrichment ($U_{(< 0.45\ \mu m)}/U_{(< 3kda)}$) and total Fe in the < 0.45 μm fraction (Fig. 3A). Moreover, if U enrichment in the < 0.45 μm fraction is driven by adsorption on Fe colloids, a positive correlation between U enrichment and Fe enrichment ($Fe_{(< 0.45\mu m)}/Fe_{(< 3kDa)}$) would be expected. However, a negative correlation was observed ($r^2 = 0.41$; n = 6; p > 0.05; Fig. 3B), but not statistically significant. These observations suggest that Fe colloids may not be the primary driver controlling the U enrichment in the < 0.45 μm fraction of groundwater. On the other hand, positive trends were observed between both U concentration and TOC in the < 0.45 μm fraction with U enrichment ($r^2 = 0.44$ and 0.57, respectively; Fig. 3C,D). Also, U concentrations are strongly associated with TOC in the < 0.45 μm fraction ($r^2 = 0.87$; n = 6; p < 0.05; Fig. 3E). These associations imply that samples with high U and high TOC exhibit greater enrichment of U in the < 0.45 μm fraction relative to the < 3 kDa fraction. Overall, it is herein speculated that the complexation of U with NOM in Ogallala groundwater likely explains the

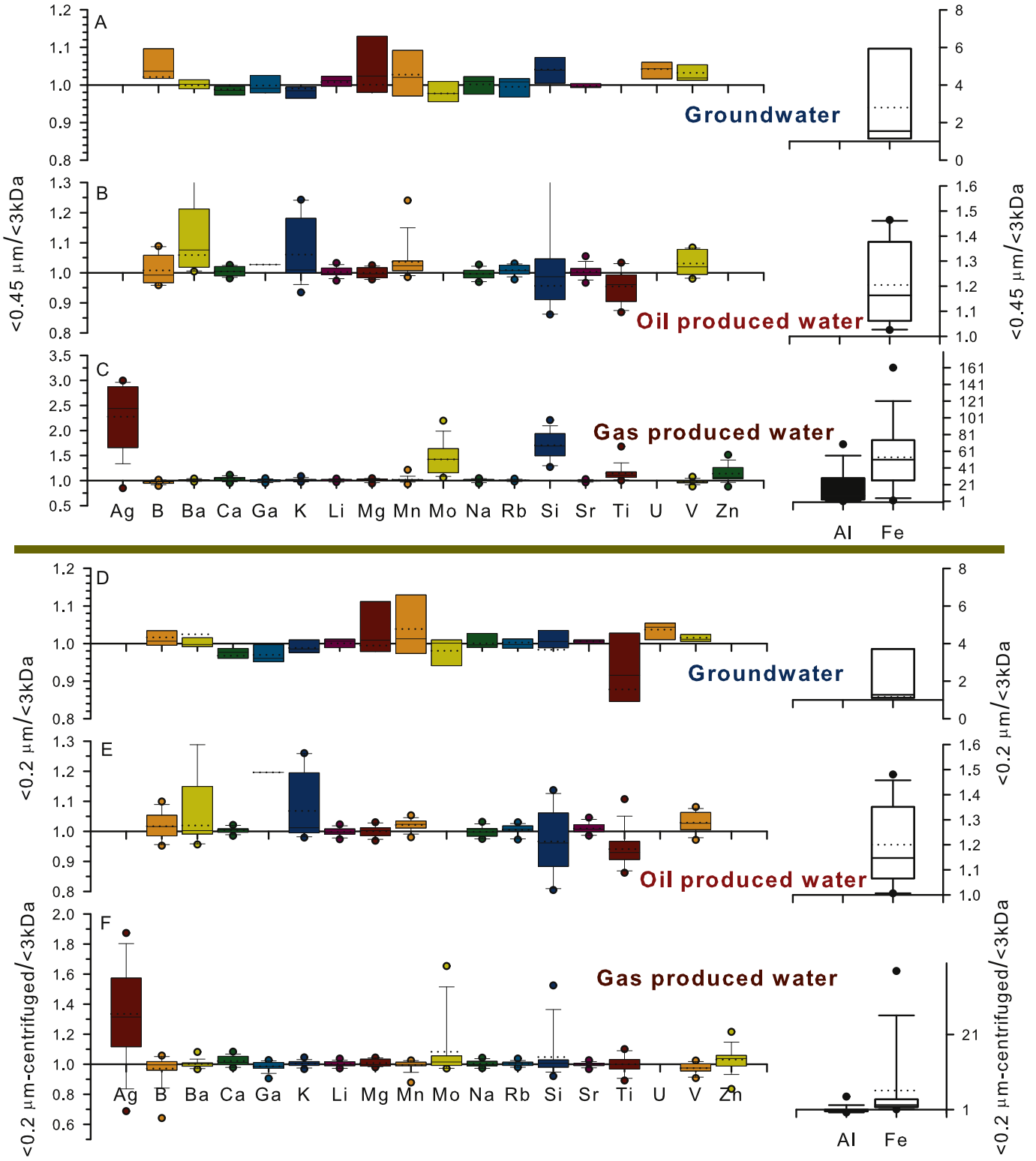

Fig. 2. Elemental ratios (< 0.45 µm fraction/ < 3 kDa fraction) and (< 0.2 µm fraction/ < 3 kDa fraction) of groundwater (A and D, respectively) and oil produced water (B and E, respectively). Elemental ratios (< 0.45 µm fraction/ < 3 kDa fraction) and (< 0.2 µm-centrifuged fraction/ < 3 kDa fraction) of natural gas produced water (C and F, respectively). Note that the scales of these plots are different. Missing box plots for some elements are because the measured concentrations of the elements were below the detection limits. Results of the statistical analysis are shown in Table 1. The elemental concentration data are reported in the supporting material (Table S1).

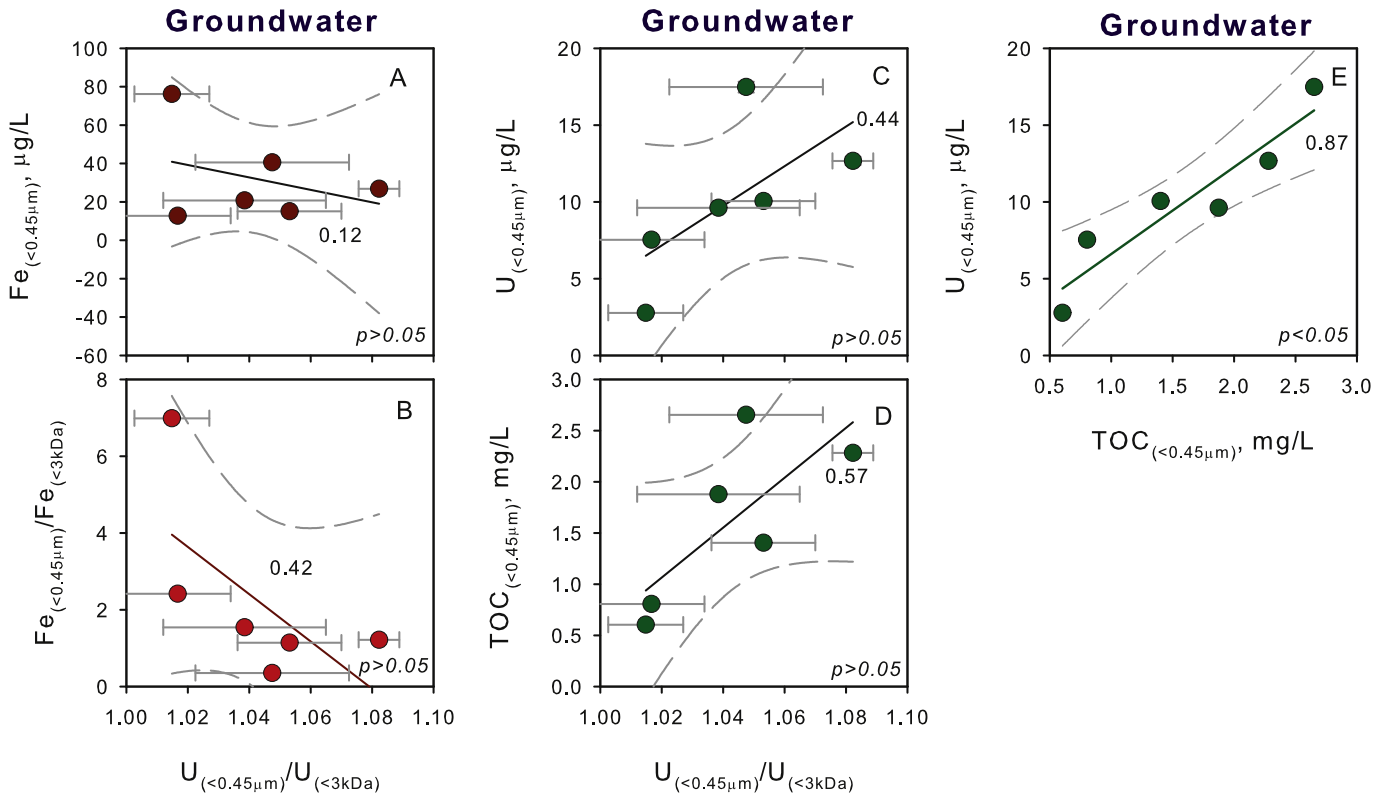

Fig. 3. Variations in Fe in the < 0.45 μm fraction (A), $Fe_{(<0.45\mu m)}/Fe_{(<3kDa)}$(B), U in the < 0.45 μm fraction (C), TOC in the < 0.45 μm fraction (D), vs. $U_{(<0.45\mu m)}/U_{(<3kDa)}$ and U vs. TOC in the < 0.45 μm fraction (E) of groundwater. The numbers between the linear regression lines (solid lines) and the 95% confidence interval lines (dashed lines; B, E) are the r^2 correlation. The error bars (1SD) for U concentration are within the size of the symbols. The error bars for $U_{(<0.45\mu m)}/U_{(<3kDa)}$ are 1SD which is calculated using equation (1) in Section 2.3.

enrichment of U in the < 0.45 μm fraction relative to U in the < 3 kDa fraction.

For oil produced water, we observed enrichment of trace metals such as Mn, Cr, and Ba (Fig. 4) in the < 0.45 μm fraction relative to the < 3 kDa fraction. A positive trend between $Cr_{(<0.45\mu m)}/Cr_{(<3kDa)}$ and $Fe_{(<0.45\mu m)}/Fe_{(<3kDa)}$ based on limited number of samples (n = 4) suggests that the dissolved Cr present in the < 0.45 μm fraction is likely adsorbed onto Fe oxyhydroxides and simultaneously removed during ultrafiltration through 3 kDa membrane. On the other hand, $Mn_{(<0.45\mu m)}/Mn_{(<3kDa)}$ and $Ba_{(<0.45\mu m)}/Ba_{(<3kDa)}$ are not correlated with $Fe_{(<0.45\mu m)}/Fe_{(<3kDa)}$, suggesting that Mn and Ba in the < 0.45 μm fraction is controlled by a different process of colloid formation. We speculate that Mn could be also oxidized to form oxides like Fe. Further, the median value of $Ba_{(0.45\mu m/3kDa)}$ (1.05; $p < 0.05$) is greater than that of $Ba_{(0.2\mu m/3kDa)}$ (1.00; $p > 0.05$)(Table 1). This suggests that the difference between Ba in the < 0.2 μm fraction and 3 kDa fraction is not significant. Waterflooding, especially re-injection of reclaimed produced water, for recovery of residual oil can promote growth of sulfate reducing microorganisms that can potentially sour the reservoirs (i.e., high concentrations of hydrogen sulfide) (Tarver and Dasgupta, 1997). Scale, particularly sulfur related scale (e.g., barite ($BaSO_4$), celestine ($SrSO_4$)), is a known issue in oil field operations (Crabtree et al., 1999). During processing of oil produced water samples, H_2S gas was evident. It is possible that oxidation of H_2S due to air exposure during syringe filtration likely causes $BaSO_4$ and $SrSO_4$ co-precipitation on the 0.2 μm membrane, explaining higher Ba in the < 0.45 μm fraction than the < 0.2 μm fraction. However, no observable difference in Sr in all three fractions was observed (Table 1). It is possible that losing Sr during syringe filtration was negligible because Sr is present at mg/L levels, much greater than Ba (ppb levels) in oil produced water. Even though no direct evidence of barite or celestine formation during syringe filtration was collected as part of this study, this hypothesis could be one of possible explanations of the enrichment of Ba in the < 0.45 μm fraction in comparison to the < 3 kDa fraction.

3.2. Naturally occurring aluminosilicate colloids in < 0.45 μm fraction of Marcellus Shale produced water

Saturation states of minerals containing Al, Si, and Ag were calculated using Geochemist's Workbench (Bethke, 2008) (thermo.com.v8r6 + thermodynamic database) for both < 0.45 μm and < 3 kDa fractions. It is noted that this non-Pitzer based thermodynamic database is used in this study because Pitzer interaction coefficients of Al, Si, and Ag are not available in other databases with the formalism of the "Pitzer equation" which are more suitable for high saline solutions. The calculated saturation indices (SI) showed that both fractions of Marcellus produced water reported in this study are oversaturated (SI > 0) with minerals relevant to Al and Si such as muscovite, montmorillonite,

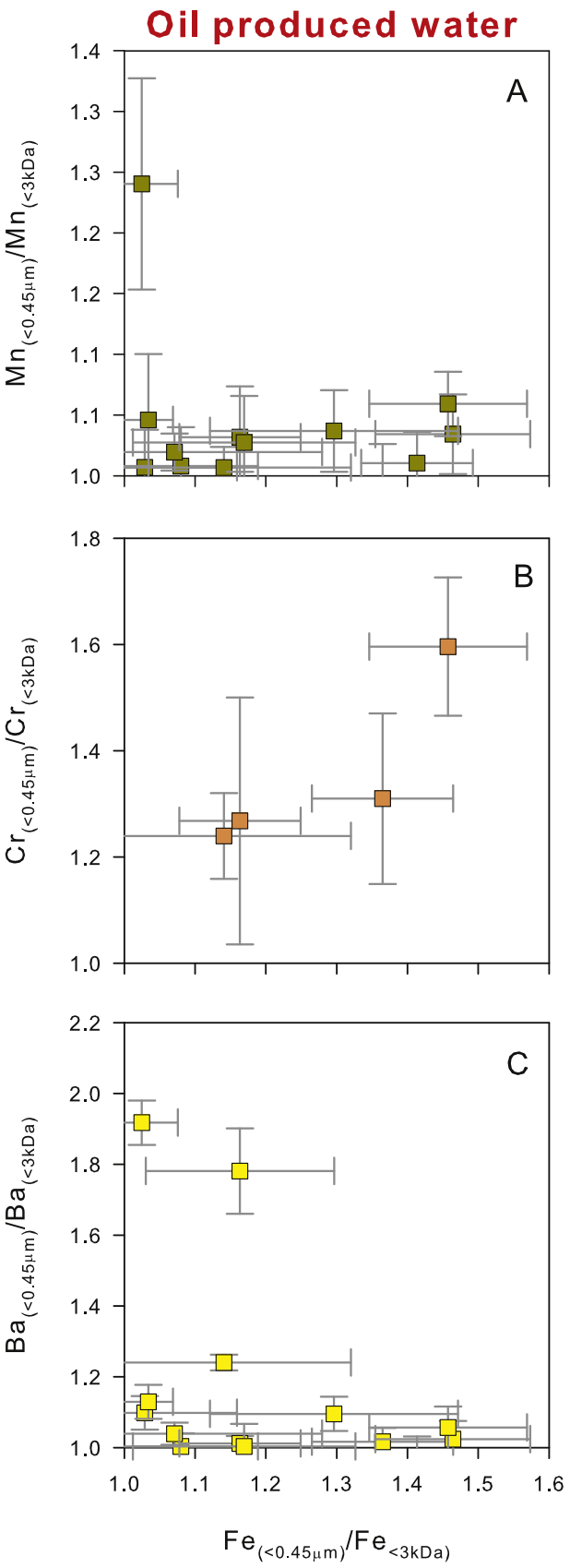

Fig. 4. Variations in $Mn_{(< 0.45\mu m)}/Mn_{(< 3kDa)}$(A), $Cr_{(< 0.45\mu m)}/Cr_{(< 3kDa)}$(B), $Ba_{(< 0.45\mu m)}/Ba_{(< 3kDa)}$ (C) vs. $Fe_{(< 0.45\mu m)}/Fe_{(< 3kDa)}$ of oil produced water. The error bars are 1SD which is calculated using equation (1) in Section 2.3.

illite, kaolinite, K-feldspar, and quartz, but undersaturated with amorphous quartz and chlorargyrite (AgCl) (Table S2). This suggests that the enrichment of Al and Si (Fig. 5A) in the < 0.45 μm fraction is likely due to the presence of aluminosilicate minerals that did not pass through a 0.2 μm membrane. Moreover, comparison of the Ti/Al (Fig. 5C) and Al/Si (Fig. 5D) ratios in colloids (calculated as follows: $Ti_{colloids}/Al_{colloids}$ = $(Ti_{(< 0.45\mu m)}\text{-}Ti_{(< 3kDa)})/(Al_{(< 0.45\mu m)}\text{-}Al_{(< 3kDa)})$ and $Al_{colloids}/Si_{colloids}$ = $(Al_{(< 0.45\mu m)}\text{-}Al_{(< 3kDa)})/(Si_{(< 0.45\mu m)}\text{-}Si_{(< 3kDa)})$) and in the three fractions with those of whole rock of Marcellus Shale (Phan et al., 2016) and clays (Mermut and Cano, 2001) reveals the colloids are close in composition to those of whole rock of Marcellus Shale and clays (Fig. 5C,D). Thus, we suggest that the presence of aluminosilicates in the < 0.45 μm fraction, possibly liberated from the rock of Marcellus Shale during hydraulic fracturing, can explain the enrichment of Al, Si, and Ti in the < 0.45 μm fraction.

Marcellus Shale is comprised of fine grains, mainly clays and quartz (Hosterman and Whitlow, 1981) generally ranging in size from submicrons to a few nanometers (Milliken et al., 2013). Clay particles were found in the sludge at the bottom of a produced water impoundment (Zhang et al., 2015), indicating 1) physical liberation during fracturing; 2) formation due to changes in temperature and/or redox potential during transport up to well head, or; 3) precipitation during impoundment storage. Results from our study ruled out the last hypothesis because clays are found in the < 0.45 μm fraction of produced water at the water-gas separator of the well. The clays likely result from either physical liberation during hydraulic fracturing or are formed during transport from the subsurface to well head, or both. In future study, inverse geochemical modeling using produced water chemistry at well head conditions may further clarify if clays are physically liberated in the subsurface or formed during transport.

We found that $Ag_{(< 0.45\mu m)}/Ag_{(< 3kDa)}$ and $Ag_{(< 0.2\mu m\text{-centrifuged})}/Ag_{(< 3kDa)}$ are significantly different from 1 ($p < 0.05$). Even though positive correlations were observed between $Ag_{(< 0.45\mu m)}/Ag_{(< 3kDa)}$ and $Ag_{(< 0.2\mu m\text{-centrifuged})}/Ag_{(< 3kDa)}$ vs. Cl (mg/L) (Fig. S1), analyzed Marcellus produced water samples are undersaturated with chlorargyrite (AgCl; Table S2). In addition, if Ag enrichment was due to the presence of colloidal AgCl, a positive correlation between $Ag_{(< 0.45\mu m)}/Ag_{(< 3kDa)}$ and $Ag_{(< 0.45\mu m)}$ would be expected; however, this correlation is very poor ($r^2 = 0.07$; Fig. S1F). This indicates that the enrichment of Ag is not likely due to the presence of colloidal chlorargyrite in the < 0.45 μm fraction. Similarly, $Ag_{(< 0.45\mu m)}/Ag_{(< 3kDa)}$ vs. $Fe_{(< 0.45\mu m)}/Fe_{(< 3kDa)}$ and $Ag_{(< 0.45\mu m)}/Ag_{(< 0.2\mu m\text{-centrifuged})}$ vs. $Fe_{(< 0.45\mu m)}/Fe_{(< 0.2\mu m\text{-centrifuged})}$ are negatively associated ($r^2 = 0.20$ and $r^2 = 0.11$, respectively) (Fig. S1D, E) indicating absorption of Ag onto Fe colloids is not the primary cause for the loss of Ag simultaneously with Fe during filtration, lowering Ag in the 3 kDa fraction. The positive correlation of $Ag_{(< 0.45\mu m)}/Ag_{(< 3kDa)}$ and $Si_{(< 0.45\mu m)}/Si_{(< 3kDa)}$ ($r^2 = 0.33$; Fig. S1G) indicates that the greater concentration of Ag in the < 0.45 μm is likely due to adsorption of Ag onto aluminosilicate colloidal materials. However, potential adsorption of Ag^+ onto the 3 kDa filter membrane (Leclerc and Wilkinson, 2013), and the 0.2 μm membrane cannot be completely ruled out.

3.3. Negligible influence of colloids on Li and radiogenic Sr isotopes

For groundwater and oil produced water, we found that there is no significant difference in $^{87}Sr/^{86}Sr$ between the < 0.45 μm, the < 0.2 μm, and the < 3 kDa fractions ($p > 0.05$; Fig. 6A and B), which is expected, because no change in Sr concentration was observed. Likewise, there is no difference in $^{87}Sr/^{86}Sr$ in the three fractions (< 0.45 μm, < 0.2 μm-centrifuged, and < 3 kDa) of gas produced water

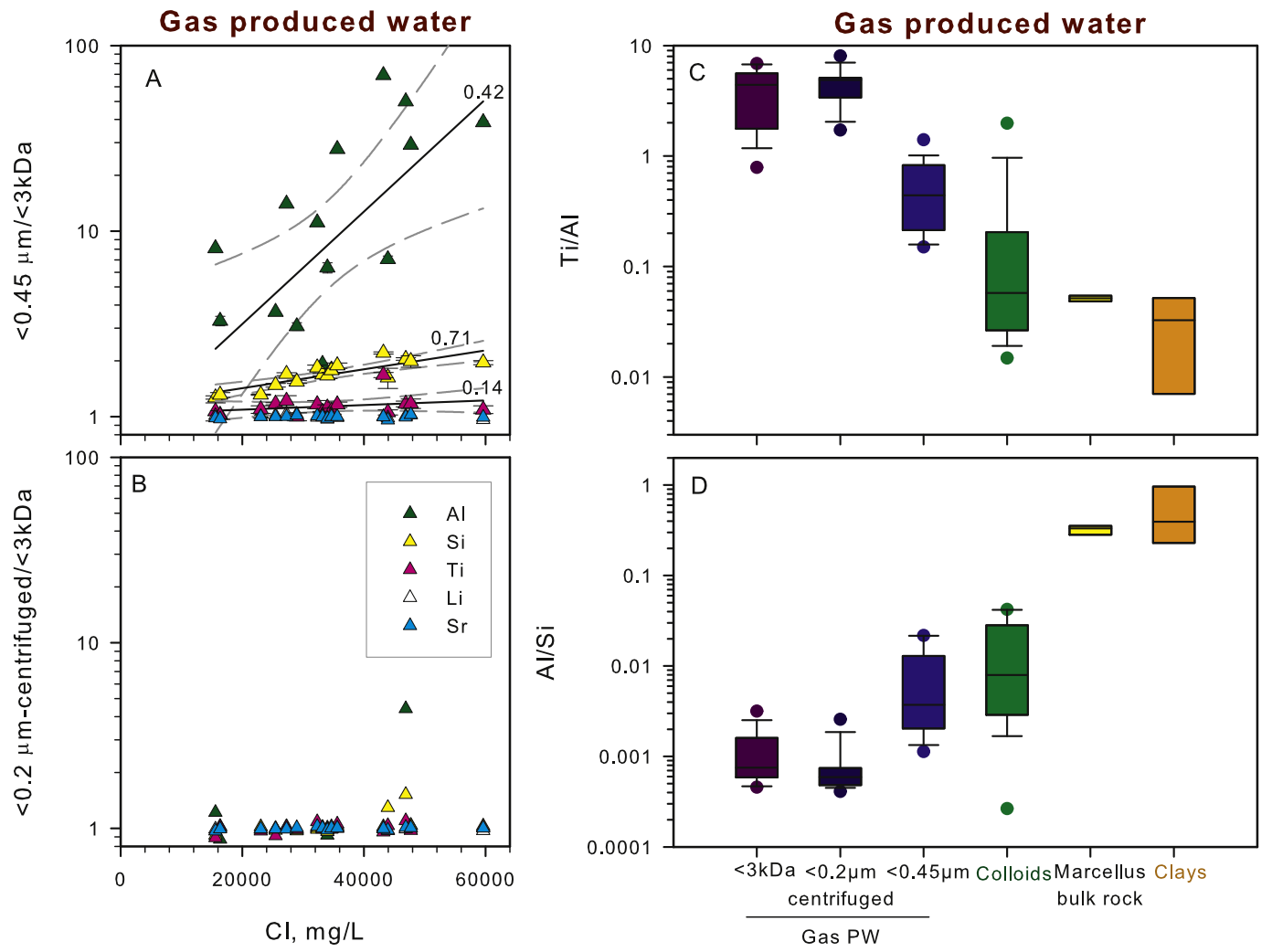

Fig. 5. Variation in elemental ratios (< 0.45 µm/ < 3 kDa)(A), (< 0.2 µm-centrifuged/ < 3 kDa)(B) vs. Cl of gas produced water. Similarity between the Ti/Al (C) and Al/Si (D) calculated ratios of colloids and bulk rock of Marcellus Shale and clays suggests the presence of aluminosilicate minerals in the < 0.45 µm fraction of Marcellus Shale produced water.

(Fig. 6 C,D). Lack of a statistically significant difference between Sr concentration in the < 0.45 µm fraction and the < 0.2 µm-centrifuged fraction ($Sr_{(<0.45\mu m)}/Sr_{(<0.2\ \mu m\text{-centrifuged})} = 1.00 \pm 0.03$; $p > 0.05$) suggests that the loss of Sr due to adsorption/co-precipitation on Fe aggregates, if it occurred, was negligible. Similarly, we found no significant difference in $^{87}Sr/^{86}Sr$ between the < 0.2 µm-centrifuged and the 3 kDa fractions, suggesting that the effect of Fe colloids on Sr isotope fractionation was also negligible.

Based on limited δ^7Li data on the gas produced water, we found that the two δ^7Li data points fall along the 1:1 line of the < 0.45 µm fraction vs. the < 0.2 µm-centrifuged fraction plot (Fig. 6E). This means that no distinguishable difference in δ^7Li between these two fractions is observed within the analytical error (0.2‰ < 2SD < 0.7‰). Even though colloidal aluminosilicate minerals are present in the < 0.45 µm fraction, but not in the < 0.2 µm-centrifuged fraction, of Marcellus Shale produced water, these colloidal clays do not significantly affect Li concentration (Table 1) or isotope composition (Fig. 6E). Because the difference in Li concentration among three fractions (< 0.45 µm, < 0.2 µm-centrifuged, and < 3 kDa) is not significant, we did not analyze the entire set of samples for δ^7Li. Li is commonly associated with clays (Phan et al., 2016; Williams and Hervig, 2005) and our previous work found that structurally bound Li in aluminosilicate minerals, particularly in clays of Marcellus Shale, accounted for 75–91% of total Li (Phan et al., 2016). Thus, colloidal clays can significantly contribute to the "dissolved" Li content and, more importantly, influence the isotope signature in colloid-rich produced water. In contrast, our results showed that the difference in Li concentration between three fractions (< 0.45 µm, < 0.2 µm-centrifuged, and < 3 kDa) is not significant (Table 1; $p > 0.05$). To illustrate, typical reproducibility for Li isotope analysis is usually around 0.5‰ (2SD; Phan et al., 2016). The difference in δ^7Li between Li in bulk rock, mainly associated with clays, (2.5 ± 2.5‰; $n = 8$) and produced water (+8 to +10‰) of Marcellus Shale is ~7‰ (Phan et al., 2016). An observable difference would require clays to contribute more than 10% of total Li in the water to be able to resolve the difference with ± 0.5‰ uncertainty.

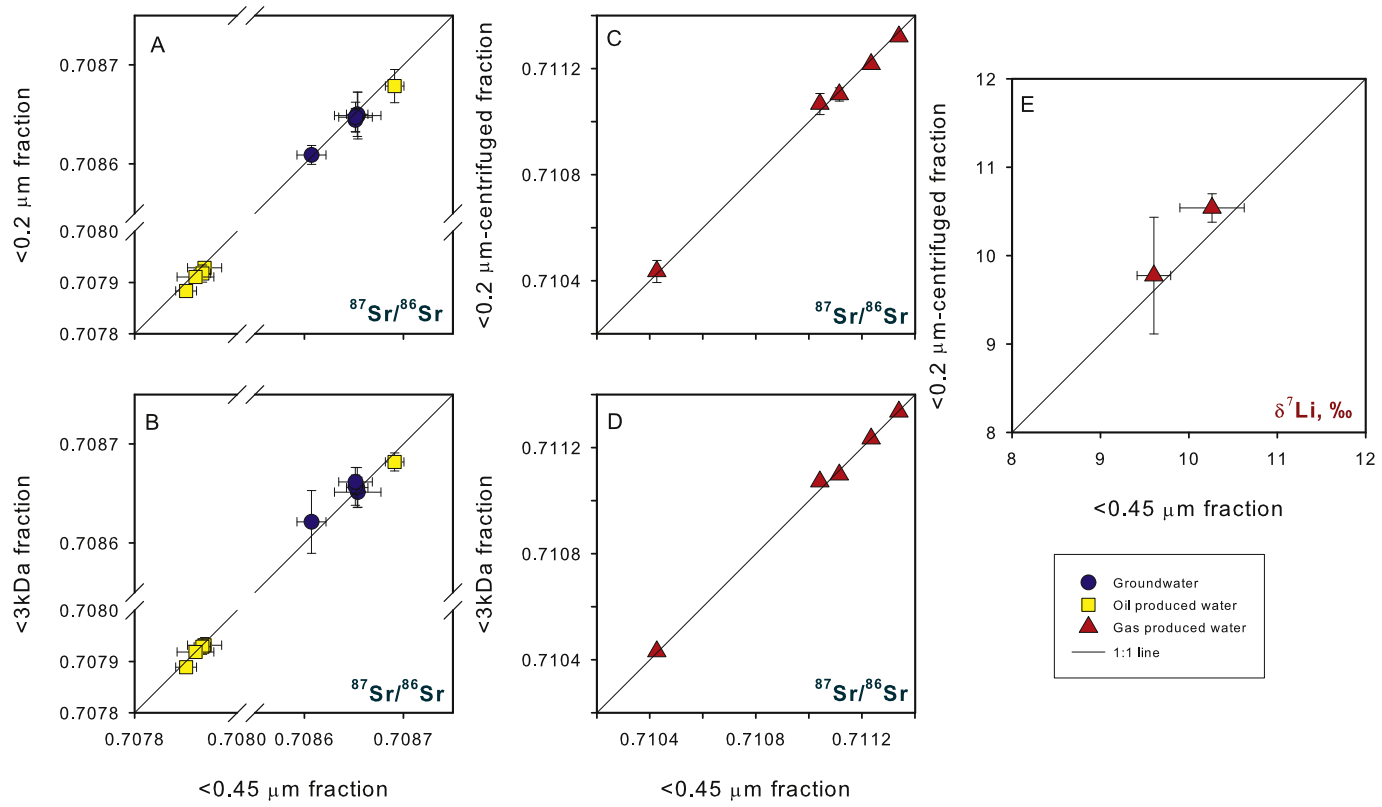

Fig. 6. Isotopic composition of Sr ($^{87}Sr/^{86}Sr$) in three fractions of groundwater and oil produced water (A,B) and gas produced water (C,D). Difference in $^{87}Sr/^{86}Sr$ between three fractions is not statistically significant ($p > 0.05$). Similarly, the difference in δ^7Li in the < 0.2 μm-centrifuged and < 0.45 μm fractions of gas produced water (E) is within the analytical error. The error bars are two standard deviations of full analytical procedure replicates (n = 3). Error bars not shown are within the size of the symbols. The isotope data for plotting this figure are shown in Table 2.

4. Conclusions

Concentrations of major (Ca, Mg, Na, K) and minor elements (e.g., Li, B, Ga, Rb, Sr) in analyzed groundwater and oil produced water filtered through a 0.45 μm membrane (< 0.45 μm fraction) do not significantly differ with the concentrations in the < 0.2 μm fraction or the < 3 kDa fraction. Likewise, the $^{87}Sr/^{86}Sr$ ratios obtained on the < 0.45 μm fraction are not significantly different with $^{87}Sr/^{86}Sr$ in the < 0.2 μm and the < 3 kDa fractions of groundwater and oil produced waters. Similar results were observed for three fractions of gas produced water (< 0.45 μm, < 0.2 μm-centrifuged, and < 3 kDa). We also found that changes in redox condition either during transport or sample collection is a primary influence on the formation of Fe colloids found in the < 0.45 μm fraction of both oil and gas produced waters. Consequently, the number of metals found to be enriched in the < 0.45 μm fraction due to the presence of colloids is greater in oil and gas produced waters than in groundwater. On the other hand, among analyzed metals in groundwater, only the enrichment of U was observed in the < 0.45 μm fraction which could be possibly explained by the complexation with organic matter.

Moreover, the presence of naturally occurring colloidal clays and quartz (aluminosilicate minerals) in the < 0.45 μm fraction of gas produced water may be entrained from the created fracture surface. Overestimation of Al, Si, and Ti, due to the presence of clays and quartz, can cause misinterpretations of water-rock interaction processes associated with clay minerals in the hydraulically fractured Marcellus Shale. Ba isotope fractionation induced by the precipitation of barite (Von Allmen et al., 2010) may occur during syringe filtration due to the oxidation of sulfide, leading to barite precipitation. Therefore, extra care should be taken when collecting sulfide rich water for barium isotope analysis. Going forward, water filtered through the 0.2 μm high capacity filter is recommended for geochemical and radiogenic Sr and Li isotopic analysis because no significant difference in metal concentrations or isotope compositions of Sr and Li was observed between < 0.2 μm and < 3 kDa fractions, and because there is low likelihood that Fe colloids or clays could influence analyses within this range of filter sizes.

Disclaimers

Any opinions, findings, conclusions, or recommendations expressed herein are those of the authors and do not necessarily reflect the views of the sponsors. Reference in this paper to any specific commercial product, process, or service is to facilitate understanding and does not imply endorsement by the United States Department of Energy.

Acknowledgements

This study was supported by the U.S. Department of Energy, Office of Fossil Energy, as part of the National Energy Technology Laboratory's ongoing research. We thank the staff of the Isotope Lab at West Virginia University for collecting the Marcellus produced water samples, field team of National Energy Technology Laboratory, Mark Garcia, John Saenz, Todd Cox, and staff with Tabula Rasa Energy for site access and aid in sample collection at the CO_2-EOR site in Seminole, TX, USA; Field access and site sampling was conducted under a MOU between NETL and Blue Strategies, LLC. The authors thank B. Stewart and R. Capo for providing clean lab space for sample preparation; M. Stuckman for assistance with TOC analysis. This research was supported in part by an appointment to the National Energy Technology Laboratory Research Participation Program, sponsored by the U.S. Department of Energy and administered by the Oak Ridge Institute for Science and Education

(TTP). The authors are grateful for constructive and helpful comments by three anonymous reviewers and careful handling of the article by the editor Thomas H. Darrah.

Appendix A. Supplementary data

Supplementary data related to this article can be found at http://dx.doi.org/10.1016/j.apgeochem.2018.05.018.

References

Andersson, P.S., Wasserburg, G.J., Ingri, J., Stordal, M.C., 1994. Strontium dissolved and particulate loads in fresh and brackish waters: the Baltic Sea and Mississippi Delta. Earth Planet Sci. Lett. 124, 195–210.

Arthur, J.D., Langhus, B.G., Patel, C., 2005. Technical Summary of Oil & Gas Produced Water Treatment Technologies.

Artinger, R., Rabung, T., Kim, J., Sachs, S., Schmeide, K., Heise, K., Bernhard, G., Nitsche, H., 2002. Humic colloid-borne migration of uranium in sand columns. J. Contam. Hydrol. 58 (1–2), 1–12.

Bažant, Z.P., Salviato, M., Chau, V.T., Viswanathan, H., Zubelewicz, A., 2014. Why fracking works. J. Appl. Mech. 81, 101010.

Bethke, C., 2008. Geochemical and Biogeochemical Reaction Modeling. Cambridge University Press Cambridge.

Bottomley, D.J., Katz, A., Chan, L.H., Starinsky, A., Douglas, M., Clark, I.D., Raven, K.G., 1999. The origin and evolution of Canadian Shield brines: evaporation or freezing of seawater? New lithium isotope and geochemical evidence from the Slave craton. Chem. Geol. 155, 295–320.

Capo, R.C., Stewart, B.W., Rowan, E.L., Kolesar Kohl, C.A., Wall, A.J., Chapman, E.C., Hammack, R.W., Schroeder, K.T., 2014. The strontium isotopic evolution of Marcellus Formation produced waters, southwestern Pennsylvania. Int. J. Coal Geol. 126, 57–63.

Chan, L.-H., Leeman, W.P., Plank, T., 2006. Lithium isotopic composition of marine sediments. G-cubed 7 (6) Q06005.

Chapman, E.C., Capo, R.C., Stewart, B.W., Kirby, C.S., Hammack, R.W., Schroeder, K.T., Edenborn, H.M., 2012. Geochemical and strontium isotope characterization of produced waters from Marcellus Shale natural gas extraction. Environ. Sci. Technol. 46, 3545–3553.

Crabtree, M., Eslinger, D., Fletcher, P., Miller, M., Johnson, A., King, G., 1999. Fighting scale—removal and prevention. Oilfield Rev. 11, 30–45.

Dellinger, M., Gaillardet, J., Bouchez, J., Calmels, D., Louvat, P., Dosseto, A., Gorge, C., Alanoca, L., Maurice, L., 2015. Riverine Li isotope fractionation in the Amazon River basin controlled by the weathering regimes. Geochem. Cosmochim. Acta 164, 71–93.

Dutton, S.P., Kim, E.M., Broadhead, R.F., Raatz, W.D., Breton, C.L., Ruppel, S.C., Kerans, C., 2005. Play analysis and leading-edge oil-reservoir development methods in the Permian basin: increased recovery through advanced technologies. AAPG Bull. 89, 553–576.

Engle, M.A., Reyes, F.R., Varonka, M.S., Orem, W.H., Ma, L., Ianno, A.J., Schell, T.M., Xu, P., Carroll, K.C., 2016. Geochemistry of formation waters from the Wolfcamp and "Cline" shales: insights into brine origin, reservoir connectivity, and fluid flow in the Permian Basin, USA. Chem. Geol. 425, 76–92.

Filella, M., 2007. Colloidal Properties of Submicron Particles in Natural Waters. IUPAC Series on Analytical and Physical Chemistry of Environmental Systems, vol. 10. pp. 17.

Harkness, J.S., Warner, N.R., Ulrich, A., Millot, R., Kloppmann, W., Ahad, J.M.E., Savard, M.M., Gammon, P., Vengosh, A., 2018. Characterization of the boron, lithium, and strontium isotopic variations of oil sands process-affected water in Alberta, Canada. Appl. Geochem. 90, 50–62.

Hosterman, J.W., Whitlow, S.T., 1981. Clay mineralogy of Devonian shales in the Appalachian basin. Geol. Surv. Open-File Rep. (United States) 81–585.

Hubbert, M.K., Willis, D.G., 1972. Mechanics of Hydraulic Fracturing.

Humez, P., Négrel, P., Lagneau, V., Lions, J., Kloppmann, W., Gal, F., Millot, R., Guerrot, C., Flehoc, C., Widory, D., Girard, J.-F., 2014. CO_2–water–mineral reactions during CO2 leakage: geochemical and isotopic monitoring of a CO_2 injection field test. Chem. Geol. 368, 11–30.

Jackson, B.P., Ranville, J.F., Bertsch, P.M., Sowder, A.G., 2005. Characterization of colloidal and humic-bound Ni and U in the "dissolved" fraction of contaminated sediment extracts. Environ. Sci. Technol. 39, 2478–2485.

Kharaka, Y.K., Maest, A.S., Carothers, W.W., Law, L.M., Lamothe, P.J., Fries, T.L., 1987. Geochemistry of metal-rich brines from central Mississippi Salt Dome basin, U.S.A. Appl. Geochem. 2, 543–561.

Košler, J., Kučera, M., Sylvester, P., 2001. Precise measurement of Li isotopes in planktonic foraminiferal tests by quadrupole ICPMS. Chem. Geol. 181 (1–4), 169–179.

Kretzschmar, R., Borkovec, M., Grolimund, D., Elimelech, M., 1999. Mobile Subsurface Colloids and Their Role in Contaminant Transport. Adv. Agron. 66, 121–193.

Kretzschmar, R., Schäfer, T., 2005. Metal retention and transport on colloidal particles in the environment. Elements 1, 205–210.

Lead, J.R., Wilkinson, K.J., 2006. Aquatic colloids and nanoparticles: current knowledge and future trends. Environ. Chem. 3, 159–171.

Leclerc, S., Wilkinson, K.J., 2013. Bioaccumulation of Nanosilver by Chlamydomonas reinhardtii – Nanoparticle or the Free Ion? Environ. Sci. Technol. 48 (1), 358–364.

Lenhart, J.J., Cabaniss, S.E., MacCarthy, P., Honeyman, B.D., 2000. Uranium (VI) complexation with citric, humic and fulvic acids. Radiochim. Acta 88, 345–354.

Macpherson, G.L., et al., 2014. Temperature-dependent Li isotope ratios in Appalachian Plateau and Gulf Coast Sedimentary Basin saline water. Geofluids 14, 419–429.

Mermut, A.R., Cano, A.F., 2001. Baseline studies of the clay minerals society source clays: chemical analyses of major elements. Clay Clay Miner. 49, 381–386.

Milliken, K.L., Rudnicki, M., Awwiller, D.N., Zhang, T., 2013. Organic matter-hosted pore system, Marcellus Formation (Devonian), Pennsylvania. AAPG (Am. Assoc. Pet. Geol.) Bull. 97, 177–200.

Pfister, S., Capo, R.C., Stewart, B.W., Macpherson, G.L., Phan, T.T., Gardiner, J.B., Diehl, J.R., Lopano, C.L., Hakala, J.A., 2017. Geochemical and lithium isotope tracking of dissolved solid sources in Permian Basin carbonate reservoir and overlying aquifer waters at an enhanced oil recovery site, northwest Texas, USA. Appl. Geochem. 87, 122–135.

Phan, T.T., Capo, R.C., Stewart, B.W., Macpherson, G., Rowan, E.L., Hammack, R.W., 2016. Factors controlling Li concentration and isotopic composition in formation waters and host rocks of Marcellus Shale, Appalachian Basin. Chem. Geol. 420, 162–179.

Phan, T.T., Paukert Vankeuren, A.N., Hakala, J.A., 2018. Roles of water–rock interactions in the geochemical evolution of Marcellus Shale produced waters. Int. J. Coal Geol. 191, 95–111.

Ranville, J.F., Hendry, M.J., Reszat, T.N., Xie, Q., Honeyman, B.D., 2007. Quantifying uranium complexation by groundwater dissolved organic carbon using asymmetrical flow field-flow fractionation. J. Contam. Hydrol. 91, 233–246.

Rowan, E.L., Engle, M.A., Kraemer, T.F., Schroeder, K.T., Hammack, R.W., Doughten, M.W., 2015. Geochemical and isotopic evolution of water produced from Middle Devonian Marcellus Shale gas wells, Appalachian Basin, Pennsylvania. AAPG (Am. Assoc. Pet. Geol.) Bull. 99, 181–206.

Tarver, G.A., Dasgupta, P.K., 1997. Oil field hydrogen sulfide in Texas: Emission estimates and fate. Environ. Sci. Technol. 31, 3669–3676.

Trostle, K.D., et al., 2016. Colloids and organic matter complexation control trace metal concentration-discharge relationships in Marshall Gulch stream waters. Water Resour. Res. 52 (10), 7931–7944.

Von Allmen, K., Böttcher, M.E., Samankassou, E., Nägler, T.F., 2010. Barium isotope fractionation in the global barium cycle: First evidence from barium minerals and precipitation experiments. Chem. Geol. 277, 70–77.

Wall, A.J., Capo, R.C., Stewart, B.W., Phan, T.T., Jain, J.C., Hakala, J.A., Guthrie, G.D., 2013. High throughput method for Sr extraction from variable matrix waters and 87Sr/86Sr isotope analysis by MC-ICP-MS. J. Anal. At. Spectrom 28, 1338–1344.

Warner, N.R., Darrah, T.H., Jackson, R.B., Millot, R., Kloppmann, W., Vengosh, A., 2014. New Tracers Identify Hydraulic Fracturing Fluids and Accidental Releases from Oil and Gas Operations. Environ. Sci. Technol. 48, 12552–12560.

Williams, L.B., Hervig, R.L., 2005. Lithium and boron isotopes in illite-smectite: The importance of crystal size. Geochem. Cosmochim. Acta 69, 5705–5716.

Wortberg, K., Conrad, S., Andersson, P.S., Ingri, J., 2017. Strontium isotopes – A tracer for river suspended iron aggregates. Appl. Geochem. 79, 85–90.

Zhang, T., Hammack, R.W., Vidic, R.D., 2015. Fate of radium in Marcellus shale flowback water impoundments and assessment of associated health risks. Environ. Sci. Technol. 49, 9347–9354.